Crystal Structure and Properties of Thallium(I) Salinomycinate

Nikolay Petkov *, Petar Dorkov, Angel Ugrinov, Elzhana Encheva, Miroslav Abrashev, Diana Zasheva, Teodora Daneva, Ivayla N. Pantcheva *

Posted Date: 24 June 2025

doi: 10.20944/preprints202506.1835.v1

Keywords: polyether ionophore; mononuclear Tl(I) complex; crystal structure; antimicrobial activity; antitumour properties

 doi:10.20944/preprints202506.1835.v1

Article

Crystal Structure and Properties of Thallium(I) Salinomycinate

Nikolay Petkov [1,*], Petar Dorkov [2], Angel Ugrinov [3], Elzhana Encheva [1], Miroslav Abrashev [4], Diana Zasheva [5], Teodora Daneva [5] and Ivayla N. Pantcheva [1,6,*]

[1] Faculty of Chemistry and Pharmacy, Sofia University "St. Kliment Ohridski", 1164 Sofia, Bulgaria
[2] Research and Development Department, Biovet Ltd., 4550 Peshtera, Bulgaria
[3] Department of Chemistry and Biochemistry, North Dakota State University, Fargo ND, USA
[4] Faculty of Physics, Sofia University "St. Kliment Ohridski", 1164 Sofia, Bulgaria
[5] Institute of Biology and Immunology of Reproduction, Bulgarian Academy of Sciences, 1113 Sofia, Bulgaria
[6] Centre of Competence "Sustainable Utilization of Bioresources and Waste of Medicinal and Aromatic Plants for Innovative Bioactive Products" (BIORESOURCES BG), 1164 Sofia, Bulgaria
* Correspondence: ahnp@chem.uni-sofia.bg (N.P.), ahip@chem.uni-sofia.bg (I.P.)

Abstract

In this study we present the preparation and characterization of novel thallium(I) coordination compound of the polyether ionophorous antibiotic salinomycin (SalH). The complex [TlSal(H_2O)] exists as two subunits SalTl1 and SalTl2 which differ slightly in their structural parameters. Salinomycin acts in a pentadentate coordination mode through oxygen donor atoms and the six-fold arrangement around the metal centers is completed by interaction with water molecule. In the overall complex structure, the two mononuclear species SalTl1 and SalTl2 are connected via hydrogen bond network by third water molecule. The inclusion of the heavy metal ion into the structure of the polyether ionophore reduces its biological activity against Gram-positive microorganisms and cervical cancer cells at *in vitro* conditions.

Keywords: polyether ionophore; mononuclear Tl(I) complex; crystal structure; antimicrobial activity; antitumour properties

1. Introduction

Salinomycinic acid (SalH, Scheme 1) is a veterinary drug used for prevention of coccidiosis in the stock farming. It belongs to the family of polyether ionophores (PIs) – natural bilogically active compounds produced by strains of *Actinomycetota* phylum (*Streptomyces* or *Actinomyces* genera). The clinically approved PIs include monensin (*Streptomyces cinnamonensins*) [1,2], salinomycin (*Streptomyces albus*) [3,4], lasalocid (*Streptomyces lasaliensis*) [5,6], narasin (*Streptomyces aureofaciens*) [7,8], maduramicin (*Actinomadura yumaensis*) [9,10], laidlomycin (*Streptomyces* spp.) and semduramicin (*Actinomadura roserufa*) [11] among over 120 polyether ionophores known today [12–14]. In addition to their coccidiostatic properties, these compounds are also used in practice as antibiotics against infections caused by Gram-positive bacteria.

 doi:10.20944/preprints202506.1835.v1

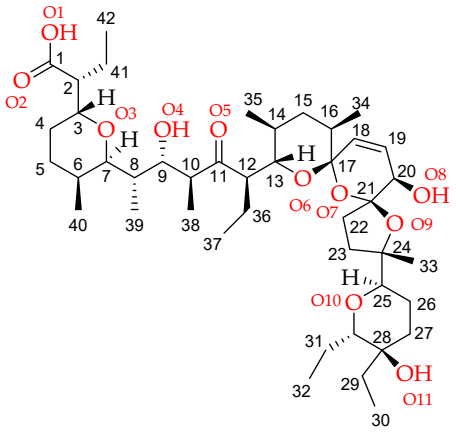

Scheme 1. Chemical structure and numbering of salinomycinic acid (SalH).

PIs are polyether derivatives of monocarboxylic acids and consist of multiple oxygen-containing heterocyclic residues linked as spiroketal fragments [15,16]. The antibiotics exist generally in a pseudo-cyclic form due to the "head-to-tail" cyclization, with most polar oxygens directed inward and with nonpolar alkyl substituents, oriented outward. The formed hydrophylic oxygen-rich cavity is able to accommodate water or monovalent metal ions [1,4,17–26]. For that reason, most of PIs possess ability to coordinate alkali metal cations as neutral complexes and are known as monovalent ion binders. However, the length of the polyether chain is responsible for the selectivity of PIs towards alkali ions (generally Na^+ *vs.* K^+) which varies depending on ionophore structure. The monovalent PIs form lipid-soluble metal complexes with group 1 metal cations, and the commercially available veterinary products contain the corresponding sodium coordination species. The neutral complexes easily penetrate through the cell membranes of sporozoites and bacteria increasing the intracellular concentration of Na^+ ions. The subsequent disturbance of metal homeostasis activates numerous energy-depending processes which result in cell death [27,28].

The binding affinity of monovalent PIs to the essential alkali cations can be further transferred to their ability to complex heavier metal(I) cations as Cs^+ or Tl^+ and in such a way – to serve as potential antidotes in the case of acute / chronic poisoning that may occur in livestock farming [29,30]. At the present we focused our study on the disposal of thallium(I), which is a nonessential element and is more toxic to the living organisms than mercury, lead and cadmium. In our study we found that the salinomycinate anion (Sal^-) binds Tl^+ ion as mononuclear coordination species (SalTl). The structure of SalTl was solved by Single Crystal X-ray Diffraction (SCXRD), and the complex was characterized by Infrared (IR) and Raman spectroscopies, mass spectrometry and elemental analysis. To the best of our knowledge, the coordination species described here are the second example of a monovalent metal derivative of the natural unmodified salinomycin, in addition to its sodium analogue [4]. Furthermore, we studied the effect of thallium(I) binding on antibacterial and antiproliferative properties of salinomycin using a set of Gram-positive bacteria and human tumour HeLa cell line (cervical cancer).

2. Results and Discussion

The interaction of salinomycinate anion (SalH, Scheme 1) with thallium(I) nitrate in a mixed solvent system leads to the spontaneous formation of mononuclear coordination species [TlSal(H_2O)] (called SalTl). The total composition of the complex can be described as [TlSal(H_2O)]×0.5H_2O due to the binding of water molecule with two SalTl subunits via hydrogen bonding. Its Time-of-Flight High-Resolution Mass Spectrum (ToF HRMS) in a positive mode (ESI+, Electro Spray Ionisation) dominates by peaks assigned to fragments containing thallium salinomycinate [SalTl]H^+ (obs. 955.4661 m/z, mass error (m.e.) 0.11 ppm), sodium salinomycinate [SalNa]H^+ (obs. 773.4819 m/z, m.e. 0.39 ppm), and Tl^+ (obs. 204.9760 m/z, m.e. 7.81 ppm).

 doi:10.20944/preprints202506.1835.v1

2.1. Description of the Crystal Structure of Thallium(I) Salinomycinate

The mononuclear SalTl complex crystalizes in space group P_1. The assymetric unit comprises two thallium(I) salinomycinates and three water molecules (Figure 1). The conformation of the two coordination species (reffered as SalTl1 and SalTl2) is practically identical with slight differences in some bond lengths and angles (Table 1). Each metal center is captured by one antibiotic monoanion through five donor atoms from bidentate carboxylate (O1, O2) and carbonyl (O5) groups, furan (O9) and pyran (O10) moieties. The sixth place in the coordination sphere of Tl^+ ions is occupied by water molecule – O1S in SalTl1 and O3S in SalTl2. The distances between thallim(I) ions and the donor atoms in both conformers vary from 2.70 to 3.33 Å and corroborate well the bond-length distribution of Tl^+ cations bonded to oxygen [31].

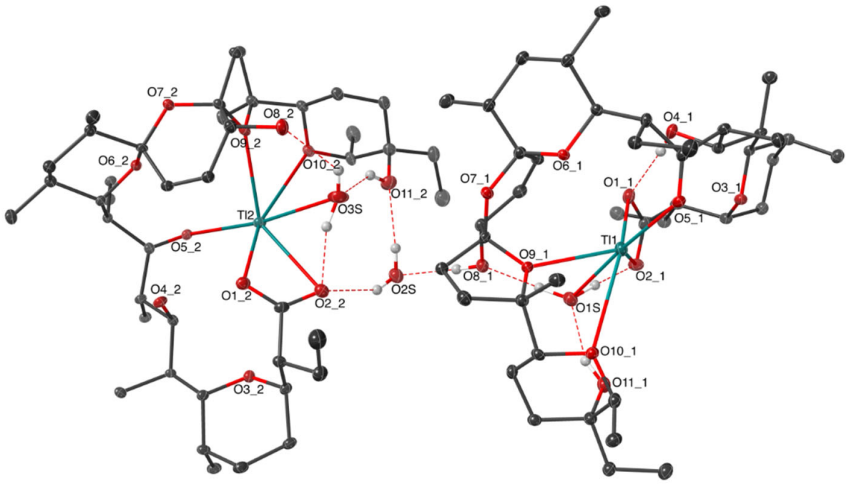

Figure 1. The asymmetric unit of SalTl with salinomycinate numbering presented in Scheme 1. Hydrogens (except those involved in H-bonds formation) are omitted for clarity. Colour code: C – grey, O – red, H – light grey, Tl – teal, H–bonds – dashed red.

Table 1. Selected bond lengths (Å) and angles (°) in the inner coordination sphere of the metal(I) cation in SalTl (n = 1 for SalTl1 and n = 2 for SalTl2).

Bond lenght	SalTl1	SalTl2
Tl – O1_n	2.742(7)	2.741(6)
Tl – O2_n	3.330(6)	3.138(6)
Tl – O5_n	2.866(5)	2.897(5)
Tl – O9_n	2.788(5)	2.724(5)
Tl – O10_n	3.266(5)	3.041(6)
Tl – O1S	2.699(6)	-
Tl – O3S	-	3.029(9)
Bond angle	**SalTl1**	**SalTl2**
O1_n – Tl – O5_n	109.5(2)	107.3(2)
O1_n – Tl – O10_n	152.6(2)	155.3(2)
O1_n – Tl – O1S	78.5(2)	-
O1_n – Tl – O3S	-	76.1(2)
O1_n – Tl – O2_n	41.9(2)	43.6(2)
O2_n – Tl – O1S	59.8(2)	-
O2_n – Tl – O3S	-	51.4(2)
O9_n – Tl – O5_n	103.6(1)	96.9(1)
O9_n – Tl – O10_n	56.4(1)	58.3(2)

 doi:10.20944/preprints202506.1835.v1

The six-fold arrangment around thallium(I) ions in the two conformers can be described as heavily distorted octahedron. The oxygens O1, O5, O10 and O1S (SalTl1) or O3S (SalTl2) and the metal center form planes with root-mean-square deviations (RMSD) of 0.077Å for Tl1 and 0.067Å for Tl2 (Figure 2). The donor atoms O2 and O9 complete the inner coordination shell, being far apart from the plane as follows: O2 – 1.490(8) Å (SalTl1), 1.573(8) Å (SalTl2); O9 – 2.268(6) Å (SalTl1), 2.246(6) Å (SalTl2). The O2–Tl–O9 angles are 119.3(1)° (SalTl1) and 125.1(2)° (SalTl2), respectively.

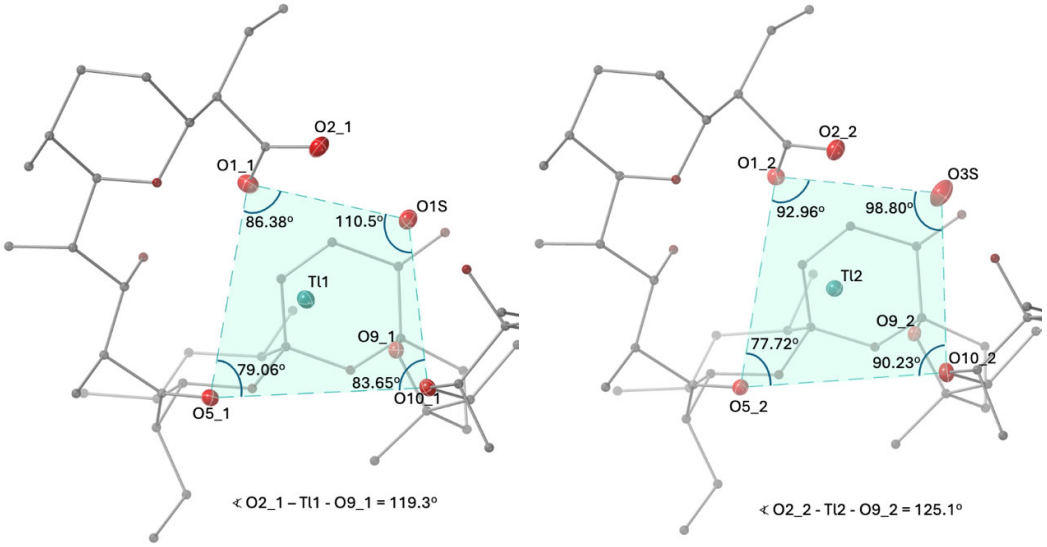

(a) (b)

Figure 2. View of the inner coordination sphere of (a) SalTl1 and (b) SalTl2 complex species.

In the individual structure of each SalTl conformer the salinomycinate exists in a "closed" form due to its "head-to-tail" folding. The hydroxyl groups O4H, O8H and O11H do not bind to the metal(I) ions, but participate in the formation of intra- and intermolecular H-bond network, which additionally stabilizes the complex units and their packing. Four internal hydrogen bonds in SalTl1 and SalTl2 are realized by interaction of O4H with O1, and O2 / O8H / O11H with O1S (SalTl1) or O3S (SalTl2). The two conformers are linked by O11_1 − O8_2 intermolecular H-bonding of 2.703 Å distance, and the water molecule O2S participates in interactions with O8H (SalTl1) and O2 / O11H (SalTl2), respectively (Table 2). The crystal packing is presented on Figure S1.

Table 2. H-bonds (Å) in SalTl (the oxygen-oxygen distances less than 3 Å are presented).

Bond	SalTl1	SalTl2
O1_n – O4_n	2.680(9)	2.720(8)
O2_n – O1S	2.602(8)	–
O2_n – O3S	–	2.675(9)
O8_n – O1S	2.718(8)	–
O8_n – O3S	–	2.684(9)
O11_n – O1S	2.672(8)	–
O11_n – O3S	–	2.651(10)
O8_n – O2S	2.714(9)	–
O2_n – O2S	–	2.848(9)
O11_n – O2S	–	2.738(9)

The existence of SalTl conformers resembles the case of sodium salinomycinate (SalNa) where the presence of two different complex species was observed (GIZDIC [4]). In contrast to the reported here thallium complex, Na^+ ions are 5- (SalNa1) or 6- (SalNa2) coordinated with the tetradentate salinomycinate anion and one (SalNa1) or two (SalNa2) water molecules, ligated to the central metal

 doi:10.20944/preprints202506.1835.v1

ion. The carboxylate group acts in a monodentate manner, and similarly to SalTl the hydroxyl groups are not directly involved in an interaction with sodium cations. In the sodium complexes of 20-deoxy (ESUZEX [21]) and 20-oxo (BIDWER [22]) derivatives of salinomycin the metal ions are 5-coordinated, with a bidentate "head" carboxylate group in the first coordination species and a "tail" hydroxyl group in the latter, without water molecules as ligands. These data highlight the role of X-ray diffraction analysis as a crucial method for determining the exact structure of complex compounds in the solid state and the conformation of the organic binder there.

The same is also true for the known thallium(I) complexes of other polyether ionophores where the antibiotics act differently. Thus, the shortest representative of PIs lasalocid forms monomer and polymer species with Tl^+ cations serving as a pentadentate ligand (JUFFOF, JUFFUL [32], JUFFOF01 [33]). Grisorixin is bound to the metal center via five O-donor atoms (GRISTL [34]), while cationomycin (BINYUS [35]) and emericid (EMERTL [36]) play as hepta- and octadentate binders, respectively. In all these complexes no water molecules are bound to the metal(I) ion, and except emericid, the carboxylate function is coordinated in a monodentate way. The Tl–O distances range from 2.60 to 3.07 Å and are in line with the data observed for the newly synthesized SalTl complex.

In addition to the SCXRD studies, we also carried out a powder XRD experiment using the bulky sample of SalTl (Figure 3). The obtained results corroborate very well the calculated pattern from the crystal structure confirming the content and purity of the entire material isolated from the crude reaction mixture. Combining the present data with those from elemental analysis (see Materials and Methods Section) and mass-spectrometry, we conclude that the bulky specimen of SalTl resembles structurally the one solved by SCXRD.

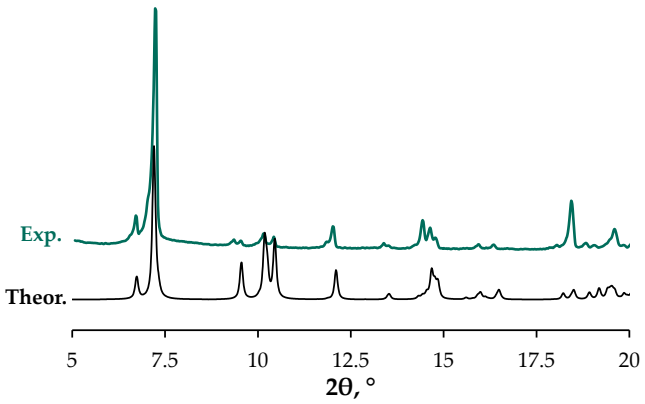

Figure 3. Calculated (black) and experimental (teal) XRD patterns of SalTl.

2.2. Spectral Characterization of SalTl

The IR spectrum of salinomycinic acid (SalH, Figure 4, Table 3) exhibits two specific bands which undergo a change upon complexation with thallium(I) ions. The first one appears as an asymmetric signal at 1709 cm^{-1} with a half-width of 40 cm^{-1}. It is assigned to the stretching vibrations of the carboxylic (1716 cm^{-1}) and the H-bonded carbonyl (1704 cm^{-1}) groups of the ligand. The second absorbance band is observed in the range of 3680-3340 cm^{-1} (centered at *ca.* 3505 cm^{-1}; half-width of 162 cm^{-1}) and is attributed to the OH-stretching vibrations within the SalH structure.

 doi:10.20944/preprints202506.1835.v1

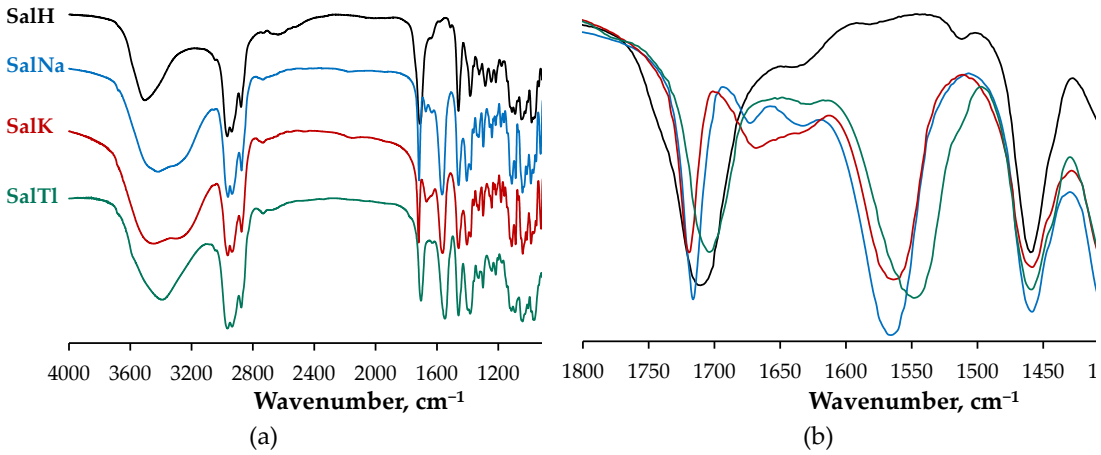

Figure 4. (a) IR spectra of SalH and its monovalent metal complexes in KBr pellets in the range 4000-400 cm^{-1}; (b) overlaid IR spectra of the studied compounds (1800-1350 cm^{-1}).

The IR spectrum of SalTl complex (Figure 4) shows some significant differences compared to that of SalH. It contains:

- a symmetric band at 1703 cm^{-1} which is narrower (half-width of 28 cm^{-1}) and less-intense due to the carbonyl stretching of the isolated C=O group, engaged in Tl-O interaction according to the X-ray findings;

- two new bands at 1549 cm^{-1} and 1398 cm^{-1} (not observable in the spectrum of SalH), which are assigned to the asymmetric and symmetric stretches of the carboxylate function. These signals evidence the deprotonation of the carboxylic group in SalH under complexation with Tl^+ cations. Furthermore, the magnitude of Δ (the difference between the two vibrations), calculated as 151 cm^{-1}, is similar but still lower than that of the corresponding ionic values, and can be used as an indicator of an asymmetric bidentate coordination mode of the carboxylate function [37]. In contrast, this difference is 161 cm^{-1} for SalNa where the carboxylate anion acts in a monodentate fashion [4], and is 159 cm^{-1} for SalK supposed to be isostructural with SalNa;

- an asymmetric broad band in the range of 3680-3120 cm^{-1} (centered at *ca*. 3390 cm^{-1}, half-width of 312 cm^{-1}), due to the OH-stretching vibrations of hydroxylic groups of salinomycinate ligand and water molecules in SalTl, engaged in the formation of Tl–O and H-bonds.

In addition to the IR study, the same set of compounds was explored by Raman spectroscopy (Figure 5) as a complementary technique to more precisely discuss some important features of SalH and its complexes with monovalent cations of Na, K and Tl. First, we were able to clearly confirm the absence of crystallinity for two of the samples evident from the broader signals observed in the Raman spectra of SalH (black) and SalK (red) due to their amorphous character. In contrast, SalNa (blue) and SalTl (teal) were examined as monocrystals apparent from the well resolved bands in the corresponding spectra. As confirmation of the crystallinity of the last two samples, the results of their study with polarized light can be considered at additional point. The observed change in the intensity of the individual bands in the Raman spectra (Figure S2) proves that the analysed samples of SalNa and SalTl are crystalline, and the crystals are larger than the spot size of the laser beam. Such behaviour of the bands in the spectra of the studied specimens of SalH and SalK is not detected from which their amorphous character can be deduced.

 doi:10.20944/preprints202506.1835.v1

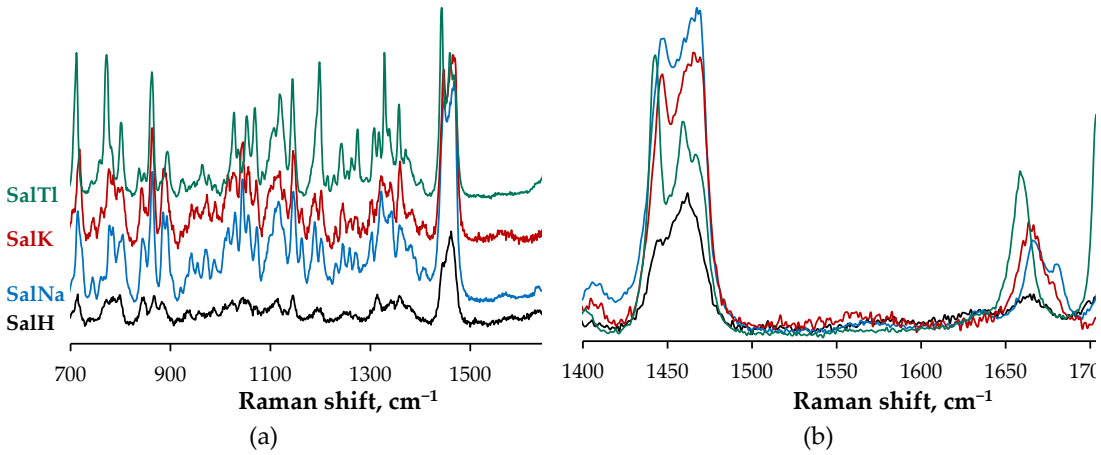

Figure 5. (a) Raman spectra of amorphous SalH and SalK, and crystalline SalNa and SalTl in 700-1750 cm^{-1} range; (b) overlaid Raman spectra of SalH and its monovalent complexes (1400-1750 cm^{-1}).

Secondly, the Raman spectroscopy allowed us to unambiguously assign the stretching vibrations of the isolated C=O and C=C bonds in SalH, which due to the higher polarizability, appear as intense signals compared to the IR spectra. Thus, we confirmed the position of the isolated C=O vibration stretch of the salinomycinic acid (Table 3) but also assigned the absorbance of its C=C vibration.

Table 3. Important IR and Raman data for SalH and complexes SalNa, SalK, SalTl.

Compound	Vibration	IR, cm^{-1}	Raman, cm^{-1}
SalH	$\nu_{C=O}$ (isolated)	1704	1705
	$\nu_{C=O}$ (COOH)	1716	–
	$\nu_{C=C}$	"hidden"	1664
SalNa	$\nu_{C=O}$ (isolated)	1716	1718, 1706
	$\nu_{C=O}$ (COO^-, asym)	1567	1570
	$\nu_{C=O}$ (COO^-, sym)	1406	–
	$\nu_{C=C}$	"hidden"	1681 / 1667
SalK	$\nu_{C=O}$ (isolated)	1719	1722
	$\nu_{C=O}$ (COO^-, asym)	1564	1560
	$\nu_{C=O}$ (COO^-, sym)	1405	–
	$\nu_{C=C}$	"hidden"	1665
SalTl	$\nu_{C=O}$ (isolated)	1703	1703
	$\nu_{C=O}$ (COO^-, asym)	1549	1555
	$\nu_{C=O}$ (COO^-, sym)	1398	–
	$\nu_{C=C}$	"hidden"	1659

In the third place, the Raman spectra show changes in the band positions due to the presence of a double bond in the structure of salinomycinate ligand. In three of the cases the band is observed as a singlet (SalH, SalK, SalTl), while in the sodium complex it is registered as a doublet arising from the Davydov splitting explained below. Looking to the spectra of three complexes, there is a clear trend that the Raman shift of C18=C19 band is proportional to the distance of the metal ion to it. Two possible explanations can be given here. From one side, the volume of the ion, which directly affects the cavity size it requires, leads to structural differences in the complexes studied. The conformation change impacts the strain in the cyclic systems, with the cyclohexenol fragment showing a difference in the value of valence angles between SalNa and SalTl coordination species (Table 4). The comparable data for SalH and SalK can be explained by the fact that salinomycin is a potassium ionophore [38] and most likely the ligand forms a cavity of similar dimension in its free and bound forms. An alternative explanation can be given by the different electronic configuration of the

 doi:10.20944/preprints202506.1835.v1

monovalent metal ions, which has been shown to affect the vibrational characteristics in unsaturated systems [39]. This can be confirmed by the position occupied by the metal ion in the structure of the complexes, which is perpendicular to the double bond allowing direct interaction with its p-orbitals.

Table 4. Bond lengths (Å) and bond angles (°) within the cyclohexenol fragment of salinomycinate in its sodium [4] and thallium complexes (subunits 1 and 2).

Band	**C17–C18**	**C18=C19**	**C19–C20**	**C20–C21**	**C21–O7**	**O7–C17**
SalNa1	1.485	1.344	1.492	1.556	1.429	1.433
SalNa2	1.472	1.311	1.420	1.566	1.435	1.429
average	1.479	1.328	1.456	1.561	1.432	1.431
SalTl1	1.507	1.318	1.497	1.522	1.419	1.431
SalTl2	1.484	1.328	1.494	1.527	1.422	1.425
average	1.500	1.323	1.500	1.525	1.421	1.428
Angle	**C17–C18–C19**	**C18=C19–C20**	**C19–C20–C21**	**C20–C21–O7**	**C21–O7–C17**	**O7–C17–C18**
SalNa1	122.1	121.0	112.4	105.7	122.4	113.0
SalNa2	123. 0	124.7	111.1	109.1	120.7	112.2
average	122.6	122.9	111.8	107.4	121.6	112.6
SalTl1	122.7	121.2	108.9	110.5	121.4	112.7
SalTl2	122.7	120.2	109.0	109.0	120.3	113.6
average	122.7	120.7	109.0	109.8	120.9	113.2

Fourth, but not least, the Raman experiment is advanced showing the clear difference between SalNa and SalTl crystals, which reflects the participation of the ligand in their inner coordination sphere according to SCXRD analysis. Thus, a strong Davydov splitting is observed in SalNa spectrum (blue) in the range of 1750-1650 cm^{-1}, much less detectable in the corresponding spectrum of SalTl (teal). This fact is attributed to the presence of two different conformers of salinomycinate ligand in the unit cell of SalNa [4], while the antibiotic anions are coordinated in a very close manner in the corresponding SalTl1 and SalTl2 complex units.

2.3. Biological Effect of SalTl and Related Compounds

The activity of SalTl on the growth of aerobic Gram-positive microorganisms was evaluated by the double layer agar diffusion assay. The choice of the laboratory strains is based on the infections caused by the bacteria against which the properties of potential drug candidates are to be tested:

- *Bacillus subtilis* (BS) is considered non-pathogenic to humans; however, it causes infections of the respiratory and urinary tracts, of dermal wounds and burns, as well as secondary nosocomial infections in immunocompromised patients [40,41];

- *Bacillus cereus* (BC) infections are associated with two types of food-borne gastroenteritis: emetic illness (due to the produced very stable toxin that is resistant to high temperatures and pH changes) and diarrhoea (mediated by a less stable enterotoxin complex) [42];

- *Kocuria rhizophila* (KR) is an outstanding example of an emerging fish pathogen [43,44] although in rare cases can be involved in human infections [45];

- *Staphylococcus aureus* (SA) is an extraordinarily versatile pathogen responsible for staphylococcal food poisoning, hospital and community-acquired infections, as well as toxic shock syndrome [46];

 doi:10.20944/preprints202506.1835.v1

- *Staphylococcus saprophyticus* (SS) causes several rare infections such as pyelonephritis, infective endocarditis, meningitis as well as urinary tract infection, endophthalmitis and uncomplicated cystitis [47].

For the sake of comparison, salinomycinic acid (SalH), monensic acid (MonH), the commercially available sodium salinomycinate (SalNa) and sodium monensinate (MonNa), as well as thallium(I) monensinate (MonTl) and $TlNO_3$ were also included in the tests. The determined minimum inhibitory concentration (MIC, μM) of the compounds assesses their ability to inhibit the visible growth of the bacterial strains. It should be borne in mind that the lower the MIC value, the better the antibacterial agent is.

Monovalent thallium ion is similar to potassium (K^+) in ionic radius and electrical charge mimicking its properties, which contributes to the toxic nature of Tl^+ *in vivo* [48] while the studies on activity of $TlNO_3$ against various bacterial strains reveals its low *in vitro* antimicrobial potential. Our data also show that thallium(I) nitrate does not inhibit the visible growth of the tested microorganisms at the highest concentration applied (1 mg/mL, 3.8 mM) except the strain of *K. rhizophila* (MIC 1.87 mM).

The antibacterial assay regarding the efficacy of ionophores and their metal derivatives outlines the following trends (Figure 6):

1) the strain of *B. cereus* (orange boxes) is the most sensitive to the effects of the tested compounds, while *K. rhizophila* (green boxes) seems to be resistant except to SalNa and SalH;

2) sodium salinomycinate (SalNa) appears to be the most toxic against the entire bacterial set, with its activity varying within a relatively narrow MIC range of 2.5-40.4 μM;

3) thallium salinomycinate (SalTl) possesses the lowest toxicity and is less active than the corresponding monensinate counterpart (MonTl).

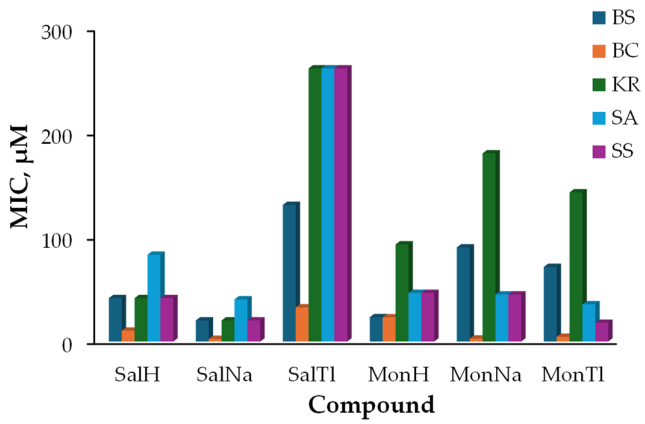

Figure 6. Minimum inhibitory concentration (MIC, μM) of SalH, MonH and their metal complexes against *B. subtilis* (BS), *B. cereus* (BS), *K. rhizophila* (KR), *S. aureus* (SA) and *S. saprophyticus* (SS).

Antibiotics and corresponding metal derivatives can be hierarchically ranked according to their decreasing inhibitory effect as follows:

BS: SalNa ≈ MonH > SalH > MonTl > MonNa > SalTl
BC: SalNa ≈ MonNa > MonTl > SalH > MonH > SalTl
KR: SalNa > SalH > MonH > MonTl > MonNa > SalTl
SA: SalNa ≈ MonTl ≈ MonNa ≈ MonH > SalH > SalTl
SS: SalNa ≈ MonTl > SalH ≈ MonNa ≈ MonH > SalTl.

The *in vitro* data obtained cannot be simply explained, as they show ambivalent trends in the effect of thallium(I) ions on the antibacterial activity of polyether ionophores. Most likely, the binding of Tl^+ to salinomycin leads to the formation of sufficiently stable coordination species that are unable to dissociate in the intracellular space of microorganisms. Thus, neither the antibiotic nor the toxic

 doi:10.20944/preprints202506.1835.v1

metal ion can exert their properties individually or synergistically. This is apparently not the case with thallium(I) monensinate, which expresses more pronounced activity, although variable across the bacterial strains tested. However, the observed differences in the susceptibility of microorganisms to structurally similar compounds indicate that each therapeutic candidate should be subjected to the most complete possible investigation of its biologically relevant properties.

To further evaluate the effect of Tl(I) ions on biological performance of salinomycin and monensin, we also conducted a pilot study using cervical cancer cells (HeLa). The HeLa were selected since they belong to one of the four female cancers diagnosed globally [49]. Unfortunately, the survival rate of patients using conventional surgery and chemotherapy is still low [50] prompting for a search of new more efficacy drugs.

The cytotoxic concentration 50 (CC_{50}, μM) of the compounds, which decreases the viability of the cells by 50% on the 24th hour after the treatment was estimated by the crystal violet (CV) assay [51]. The target ionophores, their sodium and thallium complexes, and $TlNO_3$ were applied as stock solutions in DMSO (1 mg/mL) reaching the final concentrations of 25, 10, 5, 1 and 0.5 μg/mL in working solutions using Dulbecco's Modified Eagle's Medium (DMEM) supplemented with 5% fetal bovine serum (FBS) as a dilutant. The effect of DMSO (2.5–0.05% in the respective solutions) on the proliferation of HeLa cells was found to be insignificant.

The experimental data show that the toxicity of the compounds is concentration-dependent (Figure 7), with thallium salt being again the less toxic among the studied set. The CC_{50} values of MonH and MonTl were directly determined from the dose-effect curves. The data for the others were estimated from the trendline built from the response range where a linear relationship was observed. As evident, the toxicity of SalH, SalNa and SalTl is very similar, while the compounds within the monensin series can be ordered with respect to their increasing activity as MonNa < MonH < MonTl. The diverse results observed at this stage of the modelling study appear to be due to complicated interrelationships, among which (as in the case of microbial assay) the different stability of the compounds in the specific culture medium, and therefore – their different dissociation degree is important. Based on the obtained data, we refrain to speculate on the mechanisms by which salinomycin, monensin and their metal derivatives reduce HeLa cell viability. Most likely these effects relate to the facts that i) salinomycin inhibits the growth of breast cancer (which is reproductive like cervical cancer and exhibits the same signalling pathway) [52]; ii) monensin affects various signalling pathways, including the insulin growth factor 1 receptor, essential for the development of reproductive cancer [53].

On the other hand, the observed low ability of the pure thallium(I) salt $TlNO_3$ to inhibit *in vitro* growth of microorganisms and cervical cancer cells can probably be explained by i) its ionic nature and inefficient penetration through cell membranes into the intracellular space; ii) the possibility of "blocking" negative effects by the protein components of the culture medium limiting its cellular uptake.

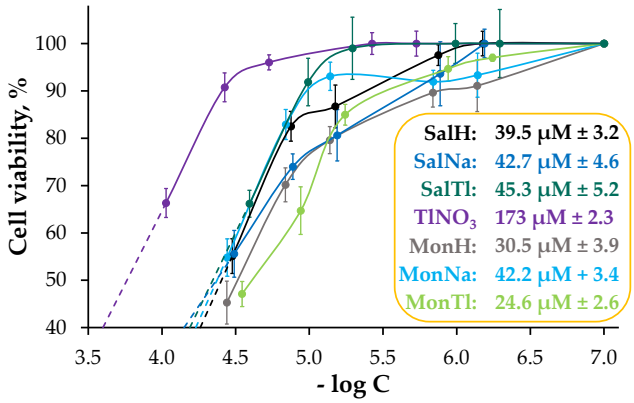

 doi:10.20944/preprints202506.1835.v1

Figure 7. Cell viability of HeLa cell line evaluated by CV assay after 24 h treatment. Inset: CC_{50} ± SD values of $TlNO_3$, salinomycin, monensin and their complexes with Na^+ and Tl^+ ions.

To obtain more detailed information about the changes in cell morphology upon treatment with the compounds studied, May-Gruenwald Giemsa (Pappenheim) staining was also performed (Figure 8). In the control group, the cells retain their normal morphology and dimensions, and no alterations in nuclear chromatin were observed. In contrast, the treatment with ionophores and their metal complexes induces remarkable changes: most cells became rounded, although the overall size is largely preserved. In cells treated with SalH, SalNa, and $TlNO_3$, the cell shape remains intact in some areas. All specimens exposed to ionophores, their metal complexes, and thallium nitrate (except SalTl) exhibit karyopyknosis, with particularly pronounced chromatin condensation observed in cells treated with SalH and MonTl. Vacuolization, a marker of cell death, is also present in some cells, especially in those exposed to MonH, its derivatives, and SalNa. Notably, SalTl-treated cells preserve their structure and size, which can be explicated by the stable complex formation and its inability to dissociate intracellularly. The observed unaffected cell morphology agrees with the low toxicity of SalTl against HeLa (CV assay) but can also be indirectly used to explain the data obtained from the antimicrobial studies.

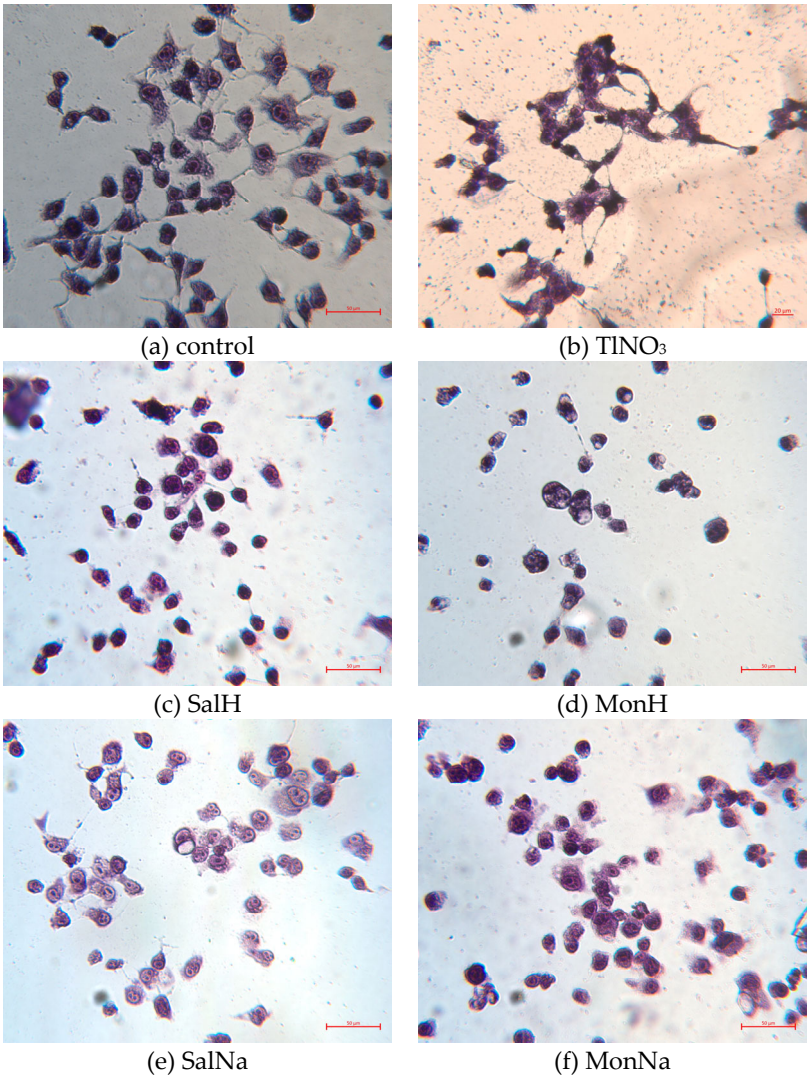

(a) control (b) $TlNO_3$

(c) SalH (d) MonH

(e) SalNa (f) MonNa

 doi:10.20944/preprints202506.1835.v1

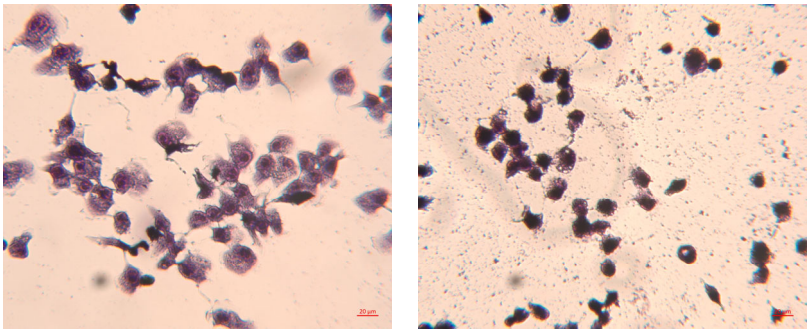

(g) SalTl (h) MonTl

Figure 8. Pappenheim staining of HeLa cells treated with $TlNO_3$, SalH, MonH and monovalent complexes at concentration of 25 μg/mL. The information in the brackets refers to the molar concentration of the compounds and the corresponding cell viability determined during the CV assay: (a) control; (b) $TlNO_3$ (93.8 μM; 66%); (c) SalH (33.3 μM; 55%); (d) MonH (36.3 μM; 45%); (e) SalNa (32.3 μM; 56%); (f) MonNa (36.1 μM; 55%); (g) SalTl (25.5 μM; 66%); (h) MonTl (28.6 μM; 47%).

In summary, we used several Gram-positive microorganisms and adherent cervical cancer cell line HeLa as model systems to evaluate the *in vitro* toxicity of monensin, salinomycin and their sodium / thallium coordination species. On the one hand, the binding of thallium ions to salinomycin reduces its bioavailability, and accordingly – its effectiveness. So, this complex is not useful as an antimicrobial and/or anticancer agent. On the other hand, the stability of SalTl discloses the potential of salinomycin for its application as a detoxifier in poisoning with thallium compounds. To confirm these initial results, additional studies are needed regarding the properties of the tested systems in solution, as well as using *in vivo* models, which are beyond the scope of the present study.

3. Materials and Methods

3.1. Reagents and Materials

Sodium salinomycinate (SalNa, p.a.) was provided by Biovet Ltd. (Huvepharma, Peshtera, Bulgaria); HCl, KOH, Et_4NOH (40% in H_2O) were purchased from Sigma-Aldrich, and $TlNO_3$, acetonitrile (MeCN), methanol (MeOH), diethyl ether (p.a. grade) were delivered from local suppliers.

The sterile plastic ware was supplied by local companies. Distilled water was used when required.

3.2. Synthesis of SalTl

A solution of $TlNO_3$ (0.2 mmol, 53.3 mg in 5 mL MeCN) was added, dropwise at constant stirring, to a solution containing SalH (0.1 mmol, 75.1 mg in 10 mL MeOH) and 0.1 mmol Et_4NOH (36 μL, 40% in H_2O). An equal volume of water (15 mL) was added to the resulting solution and allowed to evaporate slowly at room temperature. The resulting transparent colourless crystals from SalTl were washed repeatedly with water.

SalTl: $[Tl(C_{42}H_{69}O_{11})(H_2O)]\times0.5H_2O$, MW 981.41 g/mol. Elem Anal.: Calc. H, 7.40; C, 51.40%. Found: H, 7.09; C, 50.10%. Yield: 87.3 mg (88%).

3.3. X-Ray Crystallography

The crystals were mounted on a Bruker APEX-II CCD diffractometer for data collection at 107 K. The preliminary set of cells constants was calculated from the reflections collected from four sets of 30 frames which produced the initial orientation matrices. Data collection was carried out using IμS Cu Kα radiation with a detector distance of 4.0 cm. The randomly oriented region of reciprocal space was surveyed to the extent of one sphere and a resolution of 0.84 Å. Total 41 ω- and φ-scan

 doi:10.20944/preprints202506.1835.v1

sections of frames with 1.0° width were collected to achieve the desired completeness of 99.5%. The intensity data were corrected for absorption and decay [54]. The final cells constants were calculated from the xyz-centroids of the strongest reflections from the actual data collection after integration [55].

The structures were solved and refined by the SHELX [56] set of programs with Olex 2 v.1.5 software package [57]. The SHELXT [58] program was used to provide most of the non-hydrogen atoms and the full-matrix least squares/difference Fourier cycles were performed to locate the remaining non-hydrogen atoms. All non-hydrogen atoms were refined with anisotropic displacement parameters. All hydrogen atoms were placed in ideal positions and refined as riding atoms with relative isotropic displacement parameters. The data collection parameters and refinement information for the single-crystal X-ray diffraction experiments are summarized in Table 5. Images are generated using CrystalMaker Software Ltd, Oxford, England (www.crystalmaker.com).

Table 5. Crystal data and structure refinement for SalTl.

Crystal data	**SalTl**
Chemical formula	$C_{42}H_{69}O_{11}Tl \times 1.5H_2O$
M_r	981.36
Crystal system, space group	Monoclinic, P_1
Temperature (K)	107
a (Å)	12.2005(7)
b (Å)	13.7304(8)
c (Å)	14.7041(8)
α (°)	116.623(2)
β (°)	93.382(2)
γ (°)	90.454(2)
V (Å^3)	2196.6(2)
Z	2
Radiation type, λ [Å]	Cu $K\alpha$, 1.54178
μ (mm^{-1})	7.559
Crystal size (mm^3)	0.09 × 0.15 × 0.19
Data collection	
Diffractometer	Bruker APEX-II CCD
Absorption correction	Multi-scan
T_{min}, T_{max}	0.482, 0.753
No. of measured, independent and observed [$I > 2\sigma(I)$] reflections	40202, 14134, 14042
R_{int}	0.0527
Refinement	
$R[F^2 > 2\sigma(F^2)]$, $wR(F^2)$, S	0.0360, 0.0918, 1.061
No. of parameters	1033
No. of restraints	3
ΔQ_{max}, ΔQ_{min} (e Å^{-3})	2.8 (around the very heavy Tl atom)/−0.8
Absolute structure	Flack x determined using quotients [(I+)-(I–)] / [(I+)+(I–)] [59]
	0.086(7)

3.4. Physical Measurements

The powder diffraction pattern was obtained at room temperature on a PANalytical Empyrean X-ray powder diffractometer (Malvern Panalytical, Malvern, UK) with Cu Kα radiation (λ = 1.5418 Å) operating at 40 kV, 30 mA.

 doi:10.20944/preprints202506.1835.v1

IR studies in KBr pellets were performed on a Nicolet 6700 FT-IR, Thermo Scientific (Madison, WI, USA). Raman spectra were recorded on a LabRAM HR Visible Raman spectrometer in backscattering configuration (HORIBA Jobin Yvon, Kyoto, Japan). A 633 nm He-Ne laser line was used for excitation. An x50 objective was applied both to focus the incident laser light onto the sample surface and to collect the scattered light. The polarization direction of the incident linearly polarized laser light was changed using a lambda/2 plate. The scattered light was analysed with a polarizer. To avoid possible local overheating of the laser, the laser power on the laser spot (with a diameter of about 2 μm) on the sample surface was reduced to 0.5 mW.

ToF HRMS measurements were carried out on a Waters SYNAPT G2-Si Q-ToF instrument (Waters Corporation, Milford, MA, USA). The samples were dissolved in methanol and directly injected for mass spectrometry analysis in a positive ionization mode. ESI conditions were as follows: capillary potential 3.0 kV (ESI+), sample cone potential 40 V, temperature source 90 °C, desolvation temperature 250 °C, desolvation gas flow 350 L/h. The observed range was set from 50 to 2000 m/z.

The C, H analysis was performed on a Thermo Fisher Flashsmart CHN/O (Thermo Fisher Scientific, Walthman, MA, USA).

3.5. Antibacterial Activity

The Gram-positive bacteria in the present study include the strains of *Bacillus subtilis* (*BS*, NBIMCC 1050, ATCC 11774), *Bacillus cereus* (*BC*, NBIMCC 1085, ATCC 11778), *Kocuria rhizophila* (*KR*, NBIMCC 159, ATCC 9341), *Staphylococcus aureus* (*SA*, NBIMCC 509, ATCC 6538) and *Staphylococcus saprophyticus* (*SS*, NBIMCC 3348). Nutrient agar (pH 7.2-7.4) containing meat extract (3 g/L) and peptone (5 g/L) and bacterial strains were purchased from the National Bank for Industrial Microorganisms and Cell Cultures (NBIMCC, Sofia, Bulgaria).

The minimum inhibitory concentration (MIC) of compounds causing the visible inhibition of the strain's growth was determined using the double-layer agar diffusion method. Briefly, sterile (10 mL) and inoculated (10 mL, 1.5% inoculum, McFarland 4, A_{650} = 0.8−1) agar were sequentially poured onto Petri dishes (90 mm). After agar solidification, holes of 6 mm/diameter were punched and filled with 20 μL of the target compounds dissolved in MeOH. The test solutions were obtained by subsequent two-fold dilution of the stocks (1 mg/mL) up to 0.25 μg/mL. The diameter of the inhibited zones was measured after incubation at 30 °C for 24 h. Totally nine readings from three separate experiments were collected. Methanol served as a negative control. The MIC values were recalculated in μM units considering the molar mass of the tested compounds.

3.6. Cell Cultivation and Cytotoxicity Assay

The permanent cell line established from uterine cervix (HeLa, ATCC cell culture collection N CCL-2) was used as a model system in the present study. The cells were grown as monolayer cultures in Dulbecco's Modified Eagle's Medium (DMEM), supplemented with 10% fetal bovine serum (FBS), 100 U/mL penicillin and 100 μg/mL streptomycin. The culture was maintained at 37 °C in a humidified CO_2 incubator (5%). The adherent cells were detached using a mixture of 0.05% trypsin and 0.02% EDTA. The experiments were performed during the exponential phase of the cell growth. The number of vital cells was counted hemocytometrically using the trypan blue exclusion method [60].

The stock solutions of the tested compounds (1 mg/mL) were prepared in DMSO. The working solutions (25, 10, 5, 1, 0.5 μg/mL) were obtained by subsequent dilution with DMEM, supplemented with 5% FBS, 100 U/mL penicillin and 100 μg/mL streptomycin.

The cells were seeded in 96-well flat-bottomed microplates at a concentration of 1×10^4 cells per well. After growth for 24 h to a subconfluent state (~ 60−70%), the monolayers were washed with phosphate buffered saline (PBS, pH 7.2) and covered with 100 μL working solution. Each solution was applied into 4 wells. Cells grown in non-modified DMEM served as controls. After 24 h of incubation, the effect of the compounds on cell viability and proliferation was examined by crystal violet (CV) staining assay [51]. After each well was washed with PBS, the cells were fixed for 20 min

 doi:10.20944/preprints202506.1835.v1

and stained with 0.02% CV solution in methanol (100 μL) for 40 min. The excess dye was washed, and the wells were filled with 100 μL 70% ethanol (10 min) to extract the bound CV from the cells. Optical density was measured at 590 nm using an automatic microplate reader (SPECTROstar Nano, BNG Labtech, Ortenberg, Germany). Relative cell viability, expressed as a percentage of the untreated control (100% viability), was calculated for each concentration. Concentration–response curves were built and the effective cytotoxic concentration 50 of the compounds (CC_{50}, μM) was derived. All data points represent an average of three independent assays.

3.7. May-Gruenwald Giemsa (Pappenheim) Staining

HeLa cells were seeded in a 6-well plate at a density of 2×10^5 cells/well. After incubation for 24 h, the tested compounds were administered at a concentration of 25 μg/mL, and the cells were incubated again for another 24 hours. They were fixed with abs. EtOH (30-60 sec), stained subsequently with May-Grunwald and 10% Giemsa (in phosphate buffer pH 7.4) and rinsed with water. After vertical drying the morphological assessment was performed on Zeiss Axio Imager.M2 (Zeiss Group, Oberkochen, Germany).

4. Conclusions

The veterinary antibiotic salinomycin reacts with thallium(I) ion under basic conditions to form a mononuclear complex with very unsymmetric TlO_6 coordination, realized by oxygen donor atoms from pentadentate ligand monoanion and water molecule. Every two coordination species (SalTl1 and SalTl2) are linked to each other by an additional water molecule, achieving the complex composition $[TlSal(H_2O)]\times0.5H_2O$. The *in vitro* antimicrobial and antitumor assays reveal that accommodation of the heavy metal ion in the hydrophilic cavity of the ligand reduces its activity most likely due to the formation of a stable complex that is unable to dissociate in the intracellular space and disrupt the metal homeostasis of the target bacterial strains and cancer cells. The observed results can serve as a starting point for further investigation of the properties of the polyether ionophore salinomycin under different experimental conditions.

Supplementary Materials: The following supporting information can be downloaded at: Preprints.org, **Figure S1.** Crystal packing of SalTl; **Figure S2.** Comparison of the parallel and cross-polarized spectra of SalH and its complexes with Na^+, K^+ and Tl^+ ions. **CCDC 2456134** contains the supplementary crystallographic data for this paper. These data can be obtained free of charge via http://www.ccdc.cam.ac.uk (or an application from Cambridge Crystallographic Data Centre, 12 Union Road, Cambridge CB2 1EZ, UK; Fax: +44 01223 336033; or e-mail: deposit@ccdc.cam.ac.uk.

Author Contributions: Conceptualization, I.P. and N.P.; investigation, N.P., A.U., E.E., M.A., D.Z. and T.D.; resources, P.D.; writing—original draft preparation, I.P.; writing—review and editing, I.P. and N.P.; funding acquisition, I.P. All authors have read and agreed to the published version of the manuscript.

Funding: This research was funded by the European Union - NextGenerationEU, through the National Recovery and Resilience Plan of the Republic of Bulgaria, project SUMMIT BG-RRP-2.004-0008-C01 (№ 70-123-186).

Data Availability Statement: Data are available from the authors upon request.

Sample Availability: Samples of the compounds are available from the authors upon request.

Acknowledgement: Research equipment of Distributed Research Infrastructure INFRAMAT, part of Bulgarian National Roadmap for Research Infrastructures, supported by the Bulgarian Ministry of Education and Science, was used in this investigation. The support of the Centre of Competence "Sustainable Utilization of Bioresources and Waste of Medicinal and Aromatic Plants for Innovative Bioactive Products" (BIORESOURCES BG), project BG16RFPR002-1.014-0001, funded by the Program "Research, Innovation and Digitization for Smart Transformation" 2021-2027, co-funded by the EU, is greatly acknowledged.

Conflicts of Interest: Author Petar Dorkov was employed by the company Biovet Ltd. The remaining authors declare that the research was conducted in the absence of any commercial or financial relationships that could be construed as a potential conflict of interest.

 doi:10.20944/preprints202506.1835.v1

References

1. Agtarap, A.; Chamberlin, J.W.; Pinkerton, M.; Steinrauf, L. (1967) The structure of monensic acid, a new biologically active compound. *J. Am. Chem. Soc.* **1967**, *89*, 5737–5739. https://doi.org/10.1021/ja00998a062
2. Agtarap, A.; Chamberlin, J.W. Monensin, a new biologically active compound. IV. Chemistry. *Antimicrob. Agents Chemother. (Bethesda)* **1967**, *7*, 359–362. https://pubmed.ncbi.nlm.nih.gov/5596160/
3. Miyazaki, Y.; Shibuya, M.; Sugawara, H.; Kawaguchi, O.; Hirsoe, C. Salinomycin, a new polyether antibiotic. *J. Antibiotics* **1974**, *27*, 814–821. https://doi.org/10.7164/antibiotics.27.814
4. Paulus, E.F.; Kurz, M.; Matter, H.; Vértesy, L. Solid-state and solution structure of the salinomycin–sodium complex: stabilization of different conformers for an ionophore in different environments. *J. Am. Chem. Soc.* **1998**, *120*, 8209–8221. https://doi.org/10.1021/ja973607x
5. Patel, D.J.; Shen, C. Structural and kinetic studies of lasalocid A (X537A) and its silver, sodium, and barium salts in nonpolar solvents. *Proc. Natl. Acad. Sci. USA* **1976**, *73*, 1786–1790. https://doi.org/10.1073/pnas.73.6.1786
6. Erwin, G.S.; Heikkinen, J.; Pauliina Halima, P.; Haber, C.L. Streptomyces lasalocidi sp. nov. (formerly "Streptomyces lasaliensis"), an actinomycete isolated from soil which produces the polyether antibiotic lasalocid. *Intern. J. System. Evolut. Microbiol.* **2020**, *70*, 3076–3083. https://doi.org/10.1099/ijsem.0.004135
7. Berg, D.H.; Hamil, R.L. The isolation and characterization of narasin, a new polyether antibiotic. *J. Antibiot.* **1978**, *31*, 1–6. https://doi.org/10.7164/antibiotics.31.1
8. Jeffers, T.K.; Tonkinson, L.V.; Callender, M.E. Anticoccidial efficacy of narasin in battery cage trials. *Poult. Sci.* **1988**, *67*, 1043–1049. https://doi.org/10.3382/ps.0671043
9. Liu, C.M.; Hermann, T.E.; Downey, A.; Prosser, B.L.; Schildknecht, E.; Palleroni, N.J.; Westley, J.W.; Miller. P.A. Novel polyether antibiotics X-14868A, B, C, and D produced by a Nocardia. Discovery, fermentation, biological as well as ionophore properties and taxonomy of the producing culture. *J. Antibiot.* **1983**, *36*, 343–350. https://doi.org/10.7164/antibiotics.36.343
10. McDougald, L.R.; Wang, G.T.; Kantor, S.; Schenkel, R.; Quarles, C. Efficacy of maduramicin against ionophore-tolerant field isolates of coccidia in broilers. *Avian Dis.* **1987**, *31*, 302–308. https://pubmed.ncbi.nlm.nih.gov/3619823/
11. Tynan, E.J.3rd; Nelson, T.H.; Davies, R.A.; Wernau, W.C. The production of semduramicin by direct fermentation. *J. Antibiot. (Tokyo)* **1992**, *45*, 813–815. https://doi.org/10.7164/antibiotics.45.813
12. Callaway, T.R.; Edrington, T.S.; Rychlik, J.L.; Genovese, K. J.; Poole, T.L.; Jung, Y.S.; Bischoff, K.M.; Anderson, R.C; Nisbet, D.J. Ionophores: their use as ruminant growth promotants and impact on food safety. *Curr. Issues Intest. Microbiol.* **2003**, *4*, 43–51. https://pubmed.ncbi.nlm.nih.gov/14503688/
13. Novilla, M.N. Ionophores. In *Veterinary Toxicology;* Gupta, R.C., Ed.; Academic press: MA, USA, 2007, pp. 1021–1041. https://doi.org/10.1016/B978-012370467-2/50180-2
14. Dutton, C.J., Banks, B.J., Cooper, C.B. Polyether ionophores. *Nat. Prod. Rep.* **1995**, *12*, 165–181. https://doi.org/10.1039/NP9951200165
15. Riddell, F.G. Structure, conformation, and mechanism in the membrane transport of alkali metal ions by ionophoric antibiotics. *Chirality* **2002**, *14*, 121–125. https://doi.org/10.1002/chir.10052
16. Noack, S.; Chapman, H.D.; Selzer, P.M. Anticoccidial drugs of the livestock industry. *Parasitol. Res.* **2019**, *118*, 2009–2026. https://doi.org/10.1007/s00436-019-06343-5
17. Pinkerton, M.; Steinrauf, L.K. Molecular structure of monovalent metal cation complexes of monensin. *J. Mol. Biol*. **1970**, *49*, 533–546. https://doi.org/10.1016/0022-2836(70)90279-2
18. Duax, W.L.; Smith, G.D.; Strong, P.D. Complexation of metal ions by monensin. Crystal and molecular structure of hydrated and anhydrous crystal forms of sodium monensin. *J. Am. Chem. Soc.* **1980**, *102*, 6725–6729. https://doi.org/10.1021/ja00542a010
19. Pangborn, W.; Duax, W.L.; Langs, D. The hydrated potassium complex of the ionophore monensin A. *J. Am. Chem. Soc.* **1987**, *109*, 2163–2165. https://doi.org/10.1021/ja00241a038
20. Paz, F.A.A.; Gates, P.J.; Fowler, S.; Gallimore, A.; Harvey, B.; Lopes, N.P.; Stark, C.B.W.; Staunton, J.l Klinowski, J.; Spencer, J.B. Sodium monensin dihydrate. *Acta Cryst*. **2003**, *E59*, m1050–m1052. https://doi.org/10.1107/S1600536803022980

 doi:10.20944/preprints202506.1835.v1

21. Paulus, E.F.; Vértesy, L. Crystal structure of the antibiotic SY-1 (20-deoxy-salinomycin): sodium 2-(6-[2-(5-ethyl-5-hydroxy-6-methyl-tetrahydro-pyran-2-yl)-2,10,12-trimethyl-1,6,8-trioxa-dispiro[4.1.5.3]pentadec-13-en-9-yl]-2-hydroxy-1,3-dimethyl-4-oxo-heptyl-5-methyl-tetrahydro-pyran-2-yl)-butyrate—methanolsolvate (1:0.69), $C_{42}H_{69}NaO_{10} \cdot 0.69CH_3OH$. *Z. Kristallogr. NCS* **2003**, *218*, 575–577. https://doi.org/10.1524/ncrs.2003.218.4.575
22. Paulus, E.F.; Vértesy, L. Crystal structure of 2-(6-[2-(5-ethyl-5-hydroxy-6-methyl-tetrahydro-pyran-2-yl)-15-oxo-2,10,12-trimethyl-1,6,8-trioxa-dispiro[4.1.5.3]pentadec-13-en-9-yl]-2-hydroxy-1,3-dimethyl-4-oxo-heptyl-5-methyl-tetrahydro-pyran-2-yl)-butyrate sodium, $Na(C_{42}H_{67}O_{11})$, SY-9 – antibiotic 20-oxo-salinomycin. *Z. Kristallogr. NCS* **2004**, *219*, 184–186. https://doi.org/10.1524/ncrs.2004.219.14.194
23. Huczynski, A.; Ratajczak-Sitarz, M.; Katrusiak, A.; Brzezinski, B. Molecular structure of the 1:1 inclusion complex of monensin A sodium salt with acetonitrile. *J. Mol. Struct.* **2007**, *832*, 84–89. https://doi.org/10.1016/j.molstruc.2006.07.043
24. Huczynski, A.; Ratajczak-Sitarz, M.; Katrusiak, A.; Brzezinski, B. Molecular structure of the 1:1 inclusion complex of monensin A lithium salt with acetonitrile. *J. Mol. Struct.* **2007**, *871*, 92–97. https://doi.org/10.1016/j.molstruc.2006.07.046
25. Yildirim, S.O.; McKee, V.; Khardli, F.Z.; Mimouni, M.; Hadda, H.B. Rubidium(I) monensinate dihydrate. *Acta Cryst.* **2008**, *E64*, m154-m155. https://doi.org/10.1107/S1600536807065221
26. Huczynski, A.; Ratajczak-Sitarz, M.; Katrusiak, A.; Brzezinski, B. Molecular structure of rubidium six-coordinated dihydrate complex with monensin A. *J. Mol. Struct.* **2008**, *888*, 224–229. https://doi.org/10.1016/j.molstruc.2007.12.005
27. Mehlhorn, H.; Pooch, H.; Raether, W. (1983) The action of polyether ionophorous antibiotics (monensin, salinomycin, lasalocid) on developmental stages of *Eimeria tenella* (Coccidia, Sporozoa) *in vivo* and *in vitro*: study by light and electron microscopy. *Ztsch. Parasitenk.* **1983**, *69*, 457–471. https://doi.org/10.1007/BF00927702
28. Wang, Z.; Suo,X.; Xia, X.; Shen, J. Influence of monensin on cation influx and Na^+-K^+-ATPase activity of *Eimeria tenella* sporozoites in vitro. *J. Parasitol.* **2006**, *92*, 1092–1096. https://doi.org/10.1645/ge-783r.1
29. Gough, L.P.; Shacklette, H.T.; Case, A.A. Element concentrations toxic to plants, animals, and man. *Geol. Survey. Bull.* 1979, 1466, 1–78. https://doi.org/10.3133/b1466
30. Karbowska, B. Presence of thallium in the environment: sources of contaminations, distribution and monitoring methods. *Environ. Monit. Assess* **2016**, *188*, art. 640. https://doi.org/10.1007/s10661-016-5647-y
31. Gagne, O.C.; Hawthorne, F.C. Bond-length distributions for ions bonded to oxygen: metalloids and post-transition metals. *Acta Cryst.* **2018**, *B74*, 63–78. https://doi.org/10.1107/S2052252520005928
32. Aoki, K.; Suh, H.; Nagashima, H.; Uzawa, J.; Yamazaki, H. Crystal structures of two polymorphic thallium(I) salts of the antibiotic lasalocid A: a polymeric form involving metal-phenyl π-bonding and a monomeric form involving the "half-naked" metal ion. *J. Am. Chem. Soc.* **1992**, *114*, 5722–5729. https://doi.org/10.1021/ja00040a035
33. Akkurt, M.; Yıldırım, S.Ö.; Khardli, F.-Z.; Mimouni, M.; McKee, V.; Haddab, T.B. Crystal structure of a new polymeric thallium-lasalocid complex: lasalocide anion-thallium(I) containing aryl-Tl interactions. *ARKIVOC* **2008**, *xv*, 121–132. https://doi.org/10.3998/ark.5550190.0009.f13
34. Alleaume, M.; Hickel, D. Crystal structure of the thallium salt of the antibiotic grisorixin. *Chem. Comm.* **1972**, 175–176. https://doi.org/10.1039/C39720000175
35. Sakurai, T.; Kobayashi, K.; Nakamura, G.; Isono, K. Structure of the thallium salt of cationomycin. *Acta Cryst.* **1982**, *B38*, 2471–2473. https://doi.org/10.1107/S056774088200908X
36. Riche, C.; Pascard-Billy, C. Emericid-thallium(I). In Proceedings of the 3rd European Crystallographic Meeting, Zurich, Switzerland 6-10 September 1976.
37. Deacon, G.B.; Phillips, R.J. Relationships between the carbon-oxygen stretching frequencies of carboxylato complexes and the type of carboxylate coordination. *Coord. Chem. Rev.* **1980**, *33*, 227–250. https://doi.org/10.1016/S0010-8545(00)80455-5
38. Rokitskaya, T.I.; Firsov, A.M.; Khailova, L.S.; Kotova, E.A.; Antonenko, Y.N. Selectivity of cation transport across lipid membranes by the antibiotic salinomycin. *Biochim Biophys Acta Biomembr.* **2023**, *1865*, 184182. https://doi.org/10.1016/j.bbamem.2023.184182

 doi:10.20944/preprints202506.1835.v1

39. Gerasimova, T.P.; Katsyuba, S.A. Infrared and Raman bands of cyclopentadienyl ligands as indicators of electronic configuration of metal centers in metallocenes. *J. Organom. Chem.* **2015**, *776*, 30e34. https://doi.org/10.1016/j.jorganchem.2014.10.042
40. Saleh, F.; Kheirandish, F.; Azizi, H.; Azizi, M. Molecular diagnosis and characterization of *Bacillus subtilis* isolated from burn wound in Iran. *Res. Mol. Med.* **2014**, *2*, 40–44. https://doi.org/10.18869/acadpub.rmm.2.2.40
41. Loggenberg, S.R.; Twilley, D.; de Cahna, M,N.; Lall, N. Medicinal plants used in South Africa as antibacterial agents for wound healing. In *Medicinal Plants as Anti-Infectives.* Chassagne, F., Ed.; Academic Press: MA, USA, 2022; pp. 139–182. https://doi.org/10.1016/B978-0-323-90999-0.00018-5
42. Anany, H.; Brovko, L.Y.; El Arabi, T.; Griffiths, M.W. Bacteriophages as antimicrobials in food products: aApplications against particular pathogens. In *Handbook of Natural Antimicrobials for Food Safety and Quality*; Taylor, T.M., Ed.; Woodhead Publishing: Cambridge, UK, 2015; pp. 89–116. https://doi.org/10.1016/B978-1-78242-034-7.00005-0
43. Zaheen, Z.; War, A.F.; Ali, F.; Yatoo, A.M.; Ali, M.N.; Ahmad, S.B.; Rehman, M.U.; Paray, B.A. Common bacterial infections affecting freshwater fish fauna and impact of pollution and water quality characteristics on bacterial pathogenicity. *Bact. Fish Dis.* **2022**, 133–154. https://doi.org/10.1016/B978-0-323-85624-9.00006-3
44. Hajam, Y.A.; Kumar, R.; Rani, R.; Sharma, P., Diksha. Efficacy of different treatments available against bacterial pathogens in fish. *Bact. Fish Dis.* **2022**, 379–398. https://doi.org/10.1016/B978-0-323-85624-9.00013-0
45. Becker, K.; Rutsch, F.; Uekötter, A.; Kipp, F.; König, J.; Marquardt, T.; Peters, G., von Eiff, C. Kocuria rhizophila adds to the emerging spectrum of micrococcal species involved in human infections. *J. Clin. Microbiol.* **2008**, *46*, 3537–3539. https://doi.org/10.1128/JCM.00823-08
46. Castro, A.; Silva, J.; Teixeira, P. Staphylococcus aureus, a food pathogen: virulence factors and antibiotic resistance. In *Handbook of Food Bioengineering, Foodborne Diseases*; Holban, A.M.; Grumezescu, A.M., Eds.; Academic Press: MA, USA, 2018; pp. 213–238. https://doi.org/10.1016/B978-0-12-811444-5.00008-7
47. Azimi, T.; Mirzadeh, M.; Sabour, A., Nasser, A.; Fallah, F.; Pourmand, M.R. Coagulase-negative staphylococci (CoNS) meningitis: a narrative review of the literature from 2000 to 2020. *New Microbes New Infect.* **2020**, *37*, 100755. https://doi.org/10.1016/j.nmni.2020.100755
48. Toxicological review of thallium and compounds. U.S. Environmental Protection Agency, Washington, DC. EPA/635/R-08/001F; www.epa.gov/iris (accessed on April 26, 2025)
49. https://www.who.int/news-room/fact-sheets/detail/cervical-cancer (accessed on April 24, 2025).
50. Yahya, M.A.; Sharon, S.M.; Hantisteanu, S.; Hallak, M.; Bruchim, I. The role of the insulin-like growth factor 1 pathway in immune tumor microenvironment and its clinical ramifications in gynecologic malignancies. *Front. Endocrinol.* **2018**, *9*, 297. https://doi.org/10.3389/fendo.2018.00297
51. Feoktistova, M.; Geserick, P.; Leverkus, M. Crystal violet assay for determining viability of cultured cells. *Cold Spring Harb Protoc.* **2016**, 2016(4):pdb.prot087379. https://doi.org/10.1101/pdb.prot087379
52. Wang, H.; Zhang, H.; Zhu, Y.; Wu, Z.; Cui, C.; Cai, F. Anticancer mechanisms of salinomycin in breast cancer and its clinical applications. *Front. Oncol.* **2021**, *11*, 654428. https://doi.org/10.3389/fonc.2021.654428
53. Zhou, Y.; Deng, Y.; Wang, J.; Yan, Z.; Wei, Q.; Ye, J.; Zhang, J.; He, T.-C.; Qiao, M. Effect of antibiotic monensin on cell proliferation and IGF1R signaling pathway in human colorectal cancer cells. *Annals Med.* **2023**, *55*, 954–964. https://doi.org/10.1080/07853890.2023.2166980
54. *SADABS, v 2016/2 Bruker Analytical X-Ray Systems*; Bruker AXS Inc.: Madison, WI, USA, 2016.
55. *SAINTV8.38A Bruker Analytical X-Ray Systems*; Bruker AXS Inc.: Madison, WI, USA, 2018.
56. *SHELXTL 2018, Bruker Analytical X-Ray Systems*; Bruker AXS Inc.: Madison, WI, USA, 2018.
57. Dolomanov, O.V.; Bourhis, L.J.; Gildea, R.J.; Howard, J.A.; Puschmann, H.J. OLEX2: A complete structure solution, refinement and analysis program. *J. Appl. Crystallogr.* **2009**, *42*, 339–341. https://doi.org/10.1107/S0021889808042726
58. Sheldrick, G.M. SHELXT—Integrated space-group and crystal-structure determination. *Acta Cryst. A* **2015**, *71*, 3–8. https://doi.org/10.1107/S2053273314026370

 doi:10.20944/preprints202506.1835.v1

59. Parsons, S.; Flack, H.D.; Wagner, T. Use of intensity quotients and differences in absolute structure refinement. *Acta Cryst. B* **2013**, *69*, 249–259. https://doi.org/10.1107/S2052519213010014
60. Strober, W. Trypan blue exclusion test of cell viability. *Curr. Protoc. Immunol*. **2015**, *111*, A3.B.1−A3.B.3. https://doi.org/10.1002/0471142735.ima03bs111